Specific profiles of ion channels and ionotropic receptors define adipose- and bone marrow derived stromal cells

Oksana Forostyak, Olena Butenko, Miroslava Anderova, Serhiy Forostyak, Eva Sykova, Alexei Verkhratsky, G. Dayanithi

Stem Cell Research 16 (2016) 622–634

Contents lists available at ScienceDirect

Stem Cell Research

journal homepage: www.elsevier.com/locate/scr

Specific profiles of ion channels and ionotropic receptors define adipose- and bone marrow derived stromal cells

Oksana Forostyak [a,b], Olena Butenko [c,1], Miroslava Anderova [b,c], Serhiy Forostyak [b,d], Eva Sykova [b,d], Alexei Verkhratsky [e,f,g], Govindan Dayanithi [a,h,i,*]

[a] Department of Molecular Neurophysiology, Institute of Experimental Medicine, Czech Academy of Sciences, Videnska 1083, Prague 14220, Czech Republic
[b] Department of Neuroscience, Charles University, Second Faculty of Medicine, V Uvalu 84, Prague 15006, Czech Republic
[c] Department of Cellular Neurophysiology, Institute of Experimental Medicine, Czech Academy of Sciences, Videnska 1083, Prague 14220, Czech Republic
[d] Department of Neuroscience, Institute of Experimental Medicine, Czech Academy of Sciences, Videnska 1083, Prague 14220, Czech Republic
[e] University of Manchester, School of Biological Sciences, D.4417 Michael Smith Building, Oxford Road, Manchester M13 9PT, UK
[f] Achucarro Center for Neuroscience, IKERBASQUE, Basque Foundation for Science, 48011 Bilbao, Spain
[g] University of Nizhny Novgorod, Nizhny Novgorod 603022, Russia
[h] Institut National de la Santé et de la Recherche Médicale-U1198, Université Montpellier, Montpellier 34095, France
[i] Ecole Pratique des Hautes Etudes-Sorbonne, Les Patios Saint-Jacques, 4-14 rue Ferrus, 75014 Paris, France

ARTICLE INFO

Article history:
Received 13 October 2015
Received in revised form 21 March 2016
Accepted 23 March 2016
Available online 29 March 2016

Keywords:
Adipose derived stromal cells
Bone marrow stromal cell
Ca^{2+} signaling
Patch-clamp
Ion channels
Ionotropic receptors
Purinergic signaling
Ryanodine receptors
Vasopressin
Oxytocin

ABSTRACT

Adherent, fibroblastic cells from different tissues are thought to contain subsets of tissue-specific stem/progenitor cells (often called mesenchymal stem cells). These cells display similar cell surface characteristics based on their fibroblastic nature, but also exhibit differences in molecular phenotype, growth rate, and their ability to differentiate into various cell phenotypes. The mechanisms underlying these differences remain poorly understood. We analyzed Ca^{2+} signals and membrane properties in rat adipose-derived stromal cells (ADSCs) and bone marrow stromal cells (BMSCs) in basal conditions, and then following a switch into medium that contains factors known to modify their character. Modified ADSCs (mADSCs) expressed L-type Ca^{2+} channels whereas both L- and P/Q- channels were operational in mBMSCs. Both mADSCs and mBMSCs possessed functional endoplasmic reticulum Ca^{2+} stores, expressed ryanodine receptor-1 and -3, and exhibited spontaneous $[Ca^{2+}]_i$ oscillations. The mBMSCs expressed $P2X_7$ purinoceptors; the mADSCs expressed both P2X (but not $P2X_7$) and P2Y (but not $P2Y_1$) receptors. Both types of stromal cells exhibited $[Ca^{2+}]_i$ responses to vasopressin (AVP) and expressed V_1 type receptors. Functional oxytocin (OT) receptors were, in contrast, expressed only in modified ADSCs and BMSCs. AVP and OT-induced $[Ca^{2+}]_i$ responses were dose-dependent and were blocked by their respective specific receptor antagonists. Electrophysiological data revealed that passive ion currents dominated the membrane conductance in ADSCs and BMSCs. Medium modification led to a significant shift in the reversal potential of passive currents from −40 to −50 mV in cells in basal to −80 mV in modified cells. Hence membrane conductance was mediated by non-selective channels in cells in basal conditions, whereas in modified medium conditions, it was associated with K^+-selective channels. Our results indicate that modification of ADSCs and BMSCs by alteration in medium formulation is associated with significant changes in their Ca^{2+} signaling and membrane properties.

Abbreviations: α,β-MeATP, α,β-Methyleneadenosine 5′-triphosphate lithium salt; aCSF, artificial cerebrospinal fluid; ADSC, adipose derived stromal cell; AVP, arginine vasopressin; bADSC/bBMSC, ADSC/BMSC in basal conditions; bFGF, fibroblast growth factor-basic; BM, bone marrow; BMSC, bone marrow stromal cell; BzATP, 2′(3′)-O-(4-benzoylbenzoyl)adenosine 5′-triphosphate triethylammonium salt; C_m, membrane capacitance; CPA, cyclopiazonic acid; DAPI, diamidino-2-phenylindole; GABA, γ-aminobutyric acid; GVIA, ω-conotoxin GVIA; I_{KCa}, Ca^{2+}-activated K^+ channels; I_{to}, transient outward K^+ current; IK_{DR}, delayed rectifier K^+ current; IR, membrane resistance; mADCS/mBMSC, medium modified ADSC/BMSC; MVIIC, ω-conotoxin MVIIC; NMDA, N-Methyl-D-aspartic acid; OT, oxytocin; PPADS, pyridoxal phosphate-6-azo(benzene-2,4-disulfonic acid) tetrasodium salt hydrate; RA, retinoic acid; RU, ratio units; V_{rest}, resting membrane potential; VGCC, voltage-gated Ca^{2+} channels.

* Corresponding author at: Department of Molecular Neurophysiology, Institute of Experimental Medicine, Czech Academy of Sciences, Videnska 1083, CZ-14220 Prague 4, Czech Republic.
E-mail addresses: olena.butenko@unito.it (O. Butenko), gdaya@univ-montp2.fr, gdaya@biomed.cas.cz (G. Dayanithi).
[1] Present address: Neuroscience Institute Cavalieri Ottolenghi, regione Gonzole 10, 10043 Torino, Italy.

http://dx.doi.org/10.1016/j.scr.2016.03.010

1. Introduction

Adherent, fibroblastic cells from different tissues (e.g., from bone marrow, adipose tissue, umbilical cord blood, placenta, Wharton jelly, etc.) are thought to contain subsets of tissue-specific stem/progenitor cells (often called mesenchymal stem cells). These tissue-specific stem/progenitor cells share many biological features. However, they also display differences in molecular phenotype, growth rate, and their ability to differentiate into various phenotypes (Kern et al., 2006; Al-Nbaheen et al., 2013; Choudhery et al., 2013).

Calcium is a ubiquitous intracellular messenger that is a key regulator of the cell cycle, particularly during stem cell proliferation and modification. The Ca^{2+} signaling pathways have been studied in a variety of stem cell types including embryonic (Forostyak et al., 2013; Viero et al., 2014), fetal (Cocks et al., 2013) and adult stromal cells (Resende et al., 2010; Zippel et al., 2012; Kotova et al., 2014; Forostyak et al., 2016). Bone marrow stromal cells (BMSCs) have been shown to express L-type Ca^{2+} channels (Heubach et al., 2004; Li et al., 2006; Wen et al., 2012), glutamate receptors (Fox et al., 2010) and have been reported to generate spontaneous inositol 1,4,5-triphosphate ($InsP_3$)-dependent Ca^{2+} oscillations (Kawano et al., 2002, 2003). Adipose tissue-derived stromal cells (ADSCs), were found to express adrenoceptors, $InsP_3$ receptors ($InsP_3Rs$), purinoceptors and were reported to generate Ca^{2+}-induced Ca^{2+} release (Kotova et al., 2014). BMSCs have also been shown to express specific K^+ channels including Ca^{2+}-activated K^+ channels (I_{KCa}), delayed rectifier K^+ current (IK_{DR}), and transient outward K^+ current (I_{to}) (Li et al., 2006). In human BMSCs in basal conditions (bBMSCs) large conductance voltage- and Ca^{2+}-activated K^+ channels have been identified (Heubach et al., 2004). To the best of our knowledge, an in depth analysis of ion channels and receptors in ADSCs and BMSCs that have been harvested under the same environmental conditions has not been performed. In this study, we compared the functional properties of these two types of cells in basal conditions (bADSCs and bBMSCs) and after their modification (mADSCs and mADSC) induced by switching to a medium containing factors known to alter their characteristics.

2. Experimental procedures

2.1. Animals

All experiments were performed in accordance with the European Communities Council Directive of 24 November 1986 (86/609/EEC) regarding the use of animals in research, and were approved by the Ethics Committee of the Institute of Experimental Medicine, Academy of Sciences of the Czech Republic (ASCR), Prague, Czech Republic. The Sprague–Dawley rats were housed under standard laboratory conditions: a 12:12 h dark:light cycle, at 23 °C, with food and water supplied ad libitum. Bone marrow and adipose tissues used for cell isolation were collected from animals that were adequately anesthetized and subsequently euthanized.

2.2. Isolation of ADSCs

The isolation of stromal cells from adipose tissue was performed according to the protocol described previously (Arboleda et al., 2011). Adipose tissue from the inguinal pads was dissected, mechanically minced and treated with 0.2% (w/v) collagenase type I (Worthington Biochemicals, Lakewood, NJ) for 1 h at 37 °C. The isolated cellular fraction was resuspended in a proliferation medium, consisting of Dulbecco's modified Eagle's medium-DMEM/F12 + Glutamax (Gibco) supplemented with 10% fetal bovine serum and 0.2% antibiotics (primocin), and was then plated into culture flasks. Cells were harvested once they reached 90% confluence and re-plated up to the second passage. Cells from the second passage were used in their basal condition (bADSCs) or after growth in modified medium for further studies.

2.3. Isolation of BMSCs

As described previously (Forostyak et al., 2011), bone marrow (BM) was taken from femurs and tibias of 16-day-old rats. After cutting the epiphysis, BM was washed from the bones using a 2-ml syringe with a 21-gauge needle filled with DMEM containing high glucose, Glutamax 15 μl/ml (Gibco), 10% fetal calf serum and primocin 0.2%. The BM was gently dissociated and then plated into Petri dishes. The medium was changed after 24 h. When cells reached 75–90% confluence, they were detached by trypsin/EDTA treatment and transferred into culture flasks. Cells were used in their basal condition (bBMSCs) or after growth in modified medium for further studies.

2.4. Medium-modified ADSCs and BMSCs

Cultured bBMSCs or bADSCs (passage 2), after reaching 75–90% confluence, were plated at a density of 1×10^5 cells on glass bottom Petri dishes. After the attachment of the cells, the culture medium was replaced with medium consisting of a Neurobasal medium with B27 supplements containing retinoic acid (RA), 40 ng/ml, fibroblast growth factor-basic (bFGF) and 1% primocin. The cells were exposed to B27 with RA for 72 h, and then the culture media were replaced with Neurobasal medium containing B27 supplements (without RA), 40 ng/ml, bFGF and 1% primocin, and kept in culture up to 1 week. Growth factors were added every second day. The cells were measured between day 3 and day 5. This process was selected based on previous studies that explored the possibility to differentiate ADSCs into neuronal cells. Although changes in gene expression were noted, differentiation into functional neurons was not achieved (Arboleda et al., 2011).

2.5. Measurements of $[Ca^{2+}]^i$ using the fast fluorescence photometry system

$[Ca^{2+}]_i$ measurements on single cells were performed according to previously reported methods (Dayanithi et al., 1996; Forostyak et al., 2013). The cells were plated on 24 mm glass-bottom dishes (WillCo Dishes BV, Amsterdam, Netherlands) coated with laminin (Sigma-Aldrich), were incubated with 2.5 μM Fura-2 AM (Invitrogen, Carlsbad, CA, USA) with 0.02% Pluronic F-127 (Molecular Probes, Eugene, OR, USA) in culture medium at 37 °C and 5% CO_2 for 40 min. Loaded cells were then washed and the culture medium replaced with Normal Locke's buffer containing (in mM): NaCl, 140; KCl, 5; $MgCl_2$, 1.2; $CaCl_2$, 2.2; glucose, 10; HEPES-Tris, 10; pH 7.25, osmolarity 298–300 mosmol/l^{-1}) and kept at 37 °C throughout the time course of the experiment. Fluorescence measurements of $[Ca^{2+}]_i$ were performed with a fast fluorescence microspectrofluorimetry system based on an inverted microscope (Axiovert, Zeiss-Germany) equipped for epifluorescence (Plan-Neofluar 100×/1.30 oil immersion objective). To achieve fast switching between different excitation wavelengths, a rotating filter wheel was mounted in the excitation light path. The cells were illuminated (200 Hz) alternately at 340 ± 10 and 380 ± 10 nm. In order to minimize the background noise of the Fura-2 signal, successive values were averaged to a final time resolution of 320 ms. The measuring/recording amplifier was synchronized to the filter wheel to measure the fluorescence intensities resulting from different wavelengths. The FFP software controlled the acquisition of the intensity data and provided functions for adjusting the signal values as well as the display and storage of the measured data. A CCD camera was used to visualize the cells. The $[Ca^{2+}]_i$ measurement values are expressed as the ratio units (RU) between the fluorescence obtained with two excitation wavelengths, 340 nm (A) and 380 nm (B). Fura-2 calibration was performed in these cells in vitro following the procedure described previously (Lambert et al., 1994; Komori et al., 2010; Forostyak et al., 2013), which yielded $R_{min} = 0.08$, $R_{max} = 2.02$, $\beta = 1.757$. The dissociation constant for Fura-2 at 37 °C was assumed as $K_D = 224$ nM.

2.6. $[Ca^{2+}]_i$ measurements using CCD video-imaging system

$[Ca^{2+}]_i$ measurements on several cells were performed using video imaging system with an Axio Observer D1 (Zeiss) inverted microscope equipped with epifluorescence oil immersion objectives (Plan Neofluar 100× 1.30, FLUAR 40×/1.3 oil and FLUOR 20X0.75, Zeiss). The excitation light from a Xenon lamp passed through a Lambda D4 ultra-fast wavelength switching system (Sutter Instruments) with a maximum switching frequency of 500 Hz. The fluorescence intensity was detected by using a cooled CCD camera (AxioCam MRm, Zeiss) and the whole system was controlled by Zeiss ZEN Imaging software (2012-SP2/AxioVision SE64 Rel. 4.8.3). The fluorescence intensity was measured with excitations at 340 and 380 nm, and emission at 510 nm.

2.7. Drugs and solutions

Chemicals were obtained from the following companies: Sigma-Aldrich (St. Louis, MO, USA): cadmium chloride, nickel chloride, nicardipine hydrochloride, ATP, α,β-Methyleneadenosine 5′-triphosphate lithium salt (α,β-MeATP), pyridoxal phosphate-6-azo(benzene-2,4-disulfonic acid) tetrasodium salt hydrate (PPADS), 2′(3′)-O-(4-benzoylbenzoyl)adenosine 5′-triphosphate triethylammonium salt (BzATP), KN-62, L-glutamic acid potassium salt monohydrate, N-Methyl-D-aspartic acid (NMDA), γ-aminobutyric acid (GABA), adenosine, oxytocin acetate salt hydrate (OT), [Arg^8]-vasopressin acetate salt (AVP), and [deamino-Pen^1, O-Me-Tyr^2, Arg^8]-Vasopressin; Tocris Bioscience (Bristol, UK): MRS2179; NF279; Alomone Labs Ltd. (Jerusalem, Israel): ryanodine, cyclopiazonic acid (CPA), ω-conotoxin MVIIC (MVIIC), ω-conotoxin GVIA (GVIA); Phoenix Pharmaceuticals Inc.: [$d(CH_2)_5$,$Tyr(Me)^2$,Orn^8]-vasotocin ($d(CH_2)_5$OVT). Concentrated stock solutions of nicardipine, glutamate, KN-62 and ryanodine were prepared in DMSO, while the remaining stock solutions of agonists/antagonists were dissolved in dH_2O. All concentrated stock solutions were stored at −20 °C. Test solutions were prepared daily using aliquots from frozen stocks to obtain the working concentrations. All buffers and solutions in this study were made explicitly using ion-free dH_2O from Merck-Germany.

2.8. Drug application

As described previously (Dayanithi et al., 2006; Viero et al., 2006; Forostyak et al., 2013), the control and test solutions were applied using a temperature controlled multichannel polypropylene capillary perfusion system 3 (Warner Instruments, Inc., USA). The temperature of all solutions was maintained at 37 °C. After each application of the tested drug, the cells were washed with control buffer. This method allowed for fast and reliable exchange of the solution surrounding the selected cell under observation without exposing the neighboring cells.

2.9. Patch-clamp recordings

Cell membrane currents were recorded 3–4 days after the onset of differentiation using the patch-clamp technique in the whole-cell configuration. Recording pipettes with a tip resistance of 8–10 MΩ were made from borosilicate capillaries (0.86 ID, Sutter Instruments Company, Novato, CA, USA) using a P-97 Brown-Flaming micropipette puller (Sutter Instruments, Novato, CA, USA). Recording pipettes were filled with a solution containing (in mM): KCl 130, $CaCl_2$ 0.5, $MgCl_2$ 2, EGTA 5, HEPES 10. The pH was adjusted with KOH to 7.2. To visualize the recorded cells, the intracellular solution contained Alexa-Fluor hydrazide 594 (Molecular Probes, Carlsbad, CA, USA). The labeled cells were used for further post-recording immunocytochemical identification. All recordings were made in artificial cerebrospinal fluid (aCSF) containing (in mM): NaCl 122, KCl 3, $CaCl_2$ 1.5, $MgCl_2$ 1.3, Na_2HPO_4 1.25, $NaHCO_3$ 28, D-glucose 10, osmolarity 300 ± 2 mosmol/l^{-1}. The solution was continuously gassed with a mixture of 95% O_2 and 5% CO_2 to maintain a final pH of 7.4. All recordings were made on cover slips perfused with aCSF at room temperature. Electrophysiological data were measured with 10 kHz sample frequency using an EPC10 amplifier controlled by PatchMaster software (HEKA Elektronik, Lambrecht/Pfalz, Germany) and were filtered using a Bessel filter. The coverslips with cells were transferred to the recording chamber of an upright Axioscope microscope (Zeiss, Gottingen, Germany) equipped with electronic micromanipulators (Luigs & Neumann, Ratingen, Germany) and a high-resolution AxioCam HRc digital camera (Zeiss, Germany). The resting membrane potential (V_{rest}) was measured by switching the EPC-10 amplifier to the current-clamp mode.

The membrane resistance (IR) was calculated from the current elicited by a 10 mV test pulse depolarizing the cell membrane from the holding potential of −70 mV to −60 mV for 50 ms, 40 ms after the onset of the depolarizing pulse. Membrane capacitance (C_m) was determined automatically from the Lock-in protocol by PatchMaster. Current patterns were obtained by 50 ms hyper- and depolarizing the cell membrane from a holding potential of −70 mV to values ranging from −160 mV to +40 mV, at 10 mV intervals (Anderova et al., 2006; Neprasova et al., 2007). Electrophysiological data were analyzed using Fitmaster software (HEKA, Lambrecht, Germany). Membrane potentials were corrected for the liquid junction potential using JPCALCW software (Barry, 1994). After recording, the coverslips were fixed in phosphate buffer (0.2 M PB, pH 7.4) containing 4% paraformaldehyde for 15 min and then transferred to PBS (10 mM, pH 7.2).

2.10. Antibodies and immunocytochemistry

Cells plated onto laminin-coated coverslips were fixed and immunostained according to the protocol described previously (Forostyak et al., 2013). The primary and secondary antibodies used in the study are listed in Table 1. For each experiment a negative control was performed: following the same protocol, cells were blocked with normal goat serum and incubated only with secondary antibodies. To visualize the cell nuclei, following immunostaining the coverslips were incubated with 300 nM 4′,6-diamidino-2-phenylindole (DAPI) in PBS for 5 min at RT (24 °C), mounted using Aqua Poly/Mount and examined using a ZEISS LSM 510 DUO confocal microscope.

2.11. Data analysis and statistical methods

Origin 8.5.1 was employed for plotting and statistical procedures. The results are expressed as mean ± SEM. The sample size (n) given is the number of cells tested according to the same protocol (control, test drug, recovery) for each group. The figures (traces) show on-line single cell measurements of the $[Ca^{2+}]_i$ levels before and after the application of test substances, while bar diagrams and numerical data are given as mean ± S.E.M. and present the peak amplitude of the $[Ca^{2+}]_i$ increase as a ratio between the fluorescence values of 340/380 nm excitation wavelengths. Student's unpaired *t*-test or one-way ANOVA for multiple comparisons were used to determine significant differences between the experimental groups. Values of $^*p < 0.05$ and $^{**}p < 0.01$, and $^{***}p < 0.001$ were considered significant.

3. Results

3.1. $[Ca^{2+}]_i$ dynamics

The functional properties were studied using a minimum of 4 and a maximum of 10 independent cell culture preparations for both ADSCs and BMSCs. The resting level of $[Ca^{2+}]_i$ in bADSCs was 303 ± 8 nM, n = 26, and it remained stable after medium modification, being 293 ± 4 nM, n = 82 in mADSCs. In contrast, the resting $[Ca^{2+}]_i$ level in bBMSCs was significantly (p = 0.012) higher (332 ± 4 nM, n = 26) compared with bADSCs, although after medium modification, it decreased to 300 ± 8 nM, n = 49, p = 0.012 and became similar to bADSCs.

In bADSCs and bBMSCs, changes in $[Ca^{2+}]_i$ were monitored in response to a high K^+ concentration (50 mM), glutamate (100 μM), ATP

(100 μM), cyclopiasonic acid (CPA, 10 μM), oxytocin (OT, 100 nM and 1000 nM) and vasopressin (AVP, 100 nM). Both bADSCs and bBMSCs were sensitive to ATP and vasopressin, but not to the inhibitory neurotransmitters (glutamate and GABA), oxytocin or to depolarization by K^+ (Table 1). bBMSCs, but not bADSCs, were sensitive to 10 μM CPA, sarco-endoplasmic reticulum Ca^{2+}-ATP_{ase} pump inhibitor. A representative trace, showing a typical $[Ca^{2+}]_i$ response to various agonists in bBMSCs is shown in Fig. 1.

3.2. Glutamate receptors

Both bADSCs and bBMSCs did not respond to 100 μM glutamate, suggesting the absence of functional glutamate receptors (Fig. 1). Likewise the application of glutamate in mBMSCs had no effect, only one cell out of 11 showed a weak response to 100 μM glutamate. Only in mADSCs (4 out of 15 cells, 27%) glutamate at 100 mM concentration evoked a rapid $[Ca^{2+}]_i$ increase with a mean amplitude of 1.02 ± 0.22 RU. Application of 100 μM NMDA in these cells had no effect.

3.3. Voltage-gated Ca^{2+} channels

An influx of Ca^{2+} through voltage-gated Ca^{2+} channels (VGCC) is typical for excitable cells. bAMSCs and bBMSCs did not respond to depolarization by 50 mM K^+, suggesting the absence of functional VGCC in basal conditions (Table 1, Fig. 1), while after medium modification a subpopulation [46% of mADSCs (18 out of 39 cells) and 42% of mBMSCs (17 out of 41)] responded to the application of 50 mM K^+ by a rise in $[Ca^{2+}]_i$ (Table 1). The mean amplitude of this $[Ca^{2+}]_i$ increase was 1.13 ± 0.17, n = 18 in mADSCs and 0.5 ± 0.12, n = 17 in mBMSCs. Pre-incubation with Cd^{2+} (100 μM), a non-specific blocker of high-voltage activated Ca^{2+} channels, together with Ni^{2+} (50 μM), a blocker of low-voltage activated Ca^{2+} channels, for 5 min completely blocked $[Ca^{2+}]_i$ transients induced by 50 mM K^+ both in mADSCs (Fig. 2A, C) and mBMSCs (Fig. 2B, C), indicating the contributions of voltage activated Ca^{2+} channels. A selective L-type VGCC blocker, nicardipine (1 μM) completely blocked the $[Ca^{2+}]_i$ responses in 4 out of 5 tested mADSCs, while in the remaining cell, the K^+-induced $[Ca^{2+}]_i$ increase was inhibited by 34% (Fig. 2C, D). Similarly, pre-incubation of mBMSCs with nicardipine effectively blocked $[Ca^{2+}]_i$ responses in all 4 tested cells, suggesting the role for L-type Ca^{2+} channels (Fig. 2C, E). A specific P/Q-type blocker, ω-conotoxin MVIIC applied at 300 nM significantly decreased the K^+-induced $[Ca^{2+}]_i$ rise in all 6 mBMSCs tested by 61 ± 15%, p = 0.01 (Fig. 2C, G), while in mADSCs the inhibition was not significant (Fig. 2C, F). A specific N-type channel blocker ω-conotoxin GVIA (1 μM) had no effect at all both in ADSCs and BMSCs, suggesting the absence of functional N-type Ca^{2+} channels (Fig. 2C). Immunocytochemical staining revealed positive staining for L- (Fig. 2H, J, L) and P/Q-types (Fig. 2I, K, L), but not N-type VGCC (Fig. 2L) both in mADSCs and mBMSCs.

Table 1
Proportion (in %) of cells, responding to various physiological stimuli by a rise of $[Ca^{2+}]_i$ in ADSCs and BMSCs in basal and medium modified conditions.

	ADSCs		BMSCs	
	Basal	Modified	Basal	Modified
K^+ (50 mM)	0	46%	0	42%
Glutamate (100 μM)	0	27%	0	9%
GABA (50 μM)	0	0	0	0
ATP (100 μM)	90%	100%	62%	86%
CPA (1 μM)	0	100%	80%	95%
Vasopressin (100 nM)	75%	94%	100%	100%
Oxytocin (1000 nM)	0	87%	0	73%

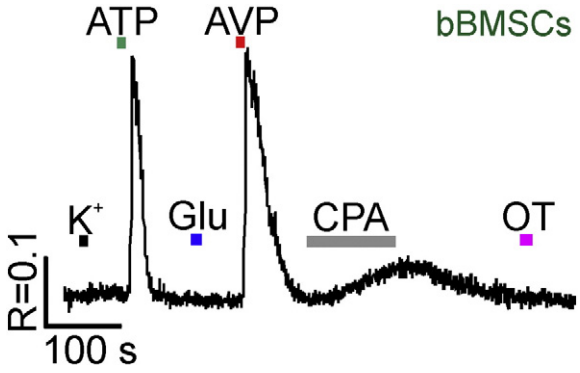

Fig. 1. Ca^{2+} measurements in BMSCs in basal conditions. A representative trace of the Ca^{2+} measurements recorded from a single bBMSC shows the typical $[Ca^{2+}]_i$ increase in response to various physiological stimuli: high K^+ (50 mM), ATP (100 μM), glutamate (100 μM), CPA (10 μM), vasopressin (AVP, 100 nM) and oxytocin (OT, 1000 nM).

3.4. Ca^{2+} release from intracellular stores and spontaneous $[Ca^{2+}]_i$ oscillations

To check the functional role of intracellular Ca^{2+} stores, we used a reversible inhibitor of sarco-endoplasmic reticulum Ca^{2+}-ATP_{ase} pump, CPA, at 10 μM. None of the 14 tested bADSCs responded to CPA, while after medium modification all 4 mADSCs tested responded to CPA by a rise of $[Ca^{2+}]_i$ with the mean amplitude of 0.62 ± 0.08 (Table 1). In contrast, both bBMSCs and mBMSCs were sensitive to CPA: 80% (16 out of 20) of bBMSCs and 92% (11 out of 12) of mBMSCs generated $[Ca^{2+}]_i$ increase (Table 1). The mean amplitude of $[Ca^{2+}]_i$ increase was 0.36 ± 0.05 (n = 16) in bBMSCs and 0.41 ± 0.04 (n = 11) in mBMSCs, respectively. Application of 2 μM ryanodine (which at this concentration activates RyRs) (Lanner et al., 2010) caused a $[Ca^{2+}]_i$ rise in 63% of the mADSCs (5 out of 8), with a mean amplitude of 1.39 ± 0.3. Immunostaining against ryanodine receptor subtypes showed that bADSCs expressed all three types (RyR1, RyR2 and RyR3) of receptors, while bBMSCs expressed mostly RyR1 and RyR3 with only a few cells positive for RyR2 (Fig. 3A). The expression of RyR1 (Fig. 3A, B, E) and RyR3 (Fig. 3A, D, G) remained unchanged or even increased in mADSCs and mBMSCs, while the expression of RyR2 in mADSCs decreased and was undetectable in mBMSCs (Fig. 3A, C, F).

Both mADSCs and mBMSCs exhibited spontaneous $[Ca^{2+}]_i$ oscillations, although only 12% of the bADSCs and none of the bBMSCs showed spontaneous $[Ca^{2+}]_i$ oscillations. A subpopulation of mADSCs (11 out of 83 cells; 13%) exhibited $[Ca^{2+}]_i$ oscillations (Fig. 3H); these were maintained after the removal of extracellular Ca^{2+}. The mean amplitude of the spontaneous $[Ca^{2+}]_i$ transients in mADSCs was 0.97 ± 0.15, the mean duration was 85.5 ± 19 s, and they appeared with a mean frequency of 4.76 mHz. About 29% of mBMSCs (14 out of 49) exhibited irregular oscillations (Fig. 3I). The mean amplitude of the spontaneous $[Ca^{2+}]_i$ transients in mBMSCs was 0.6 ± 0.14, the mean duration was 59.7 ± 9 s, and they appeared at a mean frequency of 6.94 mHz. In contrast to mADSCs, these oscillations were significantly inhibited by the application of non-specific VGCC blockers, 100 μM Cd^{2+} and 50 μM Ni^{2+} which decreased the mean amplitude of oscillations by 53 ± 12%, p = 0.001, n = 6.

3.5. Purinergic receptors

The majority of cells in basal conditions (90% (n = 22) of bADSCs and 62% (n = 26) of bBMSCs), exhibited $[Ca^{2+}]_i$ transients in response to the purinergic receptor agonist, 100 μM ATP (Table 1). The mean amplitude of $[Ca^{2+}]_i$ increase in response to 100 μM ATP in bADSCs was 2.1 ± 0.16, n = 20 and in bBMSCs was 0.83 ± 0.16, n = 16. The increase in $[Ca^{2+}]_i$ in all bBMSCs tested was significantly inhibited (98% ± 0.3%) by a non-selective P2 receptor antagonist, 10 μM PPADS (p = 0.0004, n = 5; Fig. 4A). On the contrary, in the majority of bADSCs (88%), PPADS had no effect (Fig. 4A), and only in 12% of cells tested, the ATP-

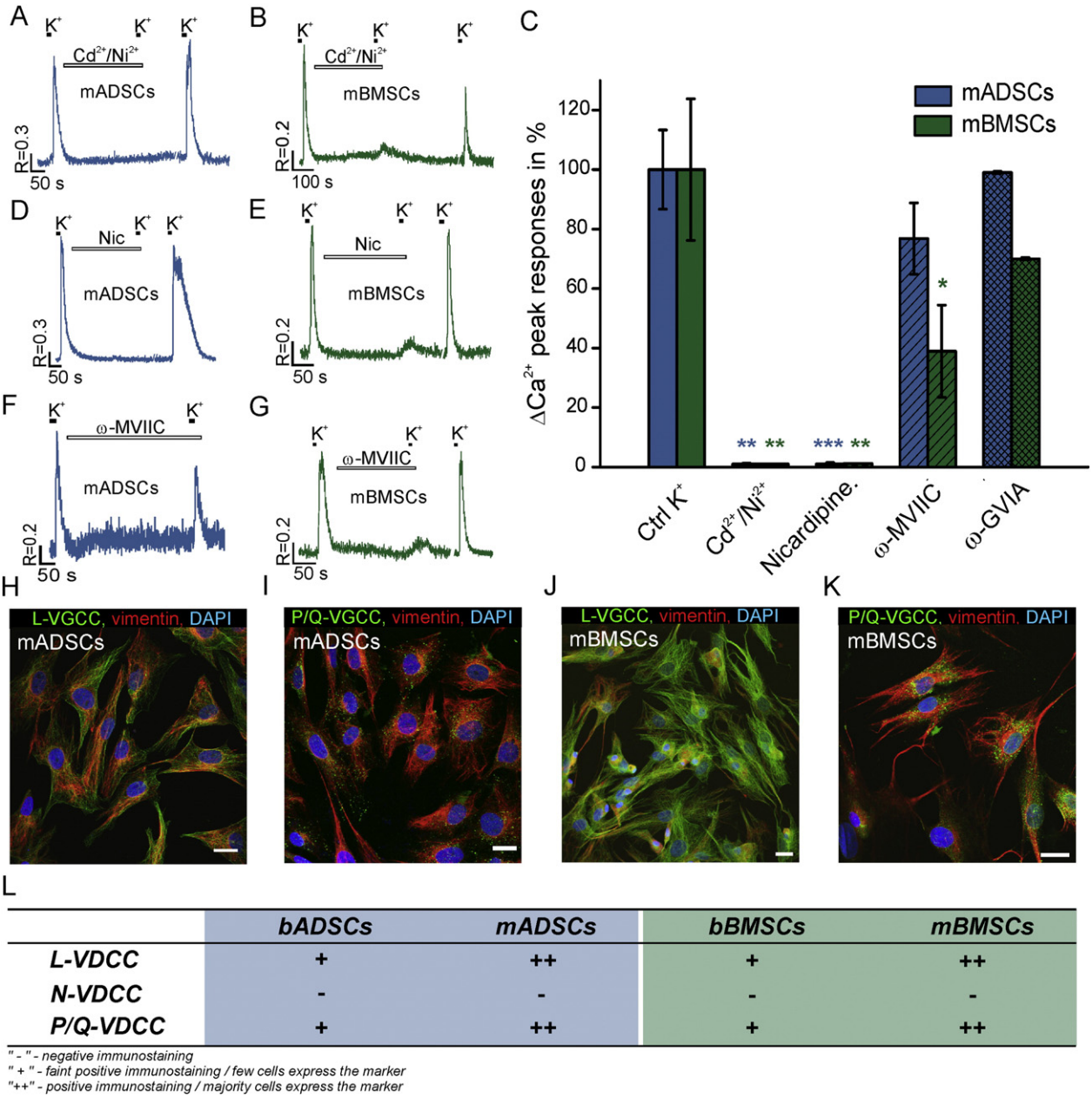

L

	bADSCs	mADSCs	bBMSCs	mBMSCs
L-VDCC	+	++	+	++
N-VDCC	-	-	-	-
P/Q-VDCC	+	++	+	++

" - " - negative immunostaining
" + " - faint positive immunostaining / few cells express the marker
"++" - positive immunostaining / majority cells express the marker

Fig. 2. Voltage-gated Ca^{2+} channels in medium-modified mADSCs and mBMSCs. Representative traces from individual mADSCs (A, D, F) and mBMSCs (B, E, G), subjected to 10 s applications 50 mM K^+ in the absence (as control stimulus) or presence (5 min duration) of Ca^{2+} channel blockers (bars) 100 μM Cd^{2+} and 50 μM Ni^{2+} (A, B), 1 μM nicardipine (D, E), 300 nM ω-conotoxin MVIIC (F, G). After the washing of blockers, the same cells were again challenged with a high K^+. C. The bar diagram represents the cumulative values (evoked peak amplitude, mean ± S.E.M) obtained from 4 to 6 cells in each of the experimental conditions, expressed as the percentage of K^+-evoked $[Ca^{2+}]_i$ responses in the absence (control) and presence of different blockers. Peak amplitude of K^+-induced $[Ca^{2+}]_i$ responses was taken as 100% (control). *$p < 0.05$; **$p < 0.01$; ***$p < 0.001$. Confocal images of mADSCs (H, I) and mBMSCs (J, K), co-stained for vimentin (red) and L-type or P/Q-type VGCC (green). Cell nuclei were visualized with DAPI staining. Scale bars = 20 μm. L. Table showing the expression of Ca^{2+} channels in basal and medium-modified ADSCs and BMSCs.

induced $[Ca^{2+}]_i$ rise was inhibited by 47% ± 4%. Other P2X antagonists KN-62 and NF279 had no effect in both bADSCs and bBMSCs.

Application of 100 μM ATP in mADSCs induced a rapid increase in $[Ca^{2+}]_i$ with a mean amplitude of 1.55 ± 0.09 in all 43 cells tested (Fig. 4B). BzATP at a 20 μM concentration (Fig. 4B) appeared to be a less potent agonist than ATP, inducing a significantly smaller increase in $[Ca^{2+}]_i$ of 0.92 ± 0.12 in 88% of cells tested (14 out of 16; $p = 0.001$). In 24% (4 out of 17) of the cells, the least potent agonist, α,β-meATP (100 μM), caused a significantly weaker $[Ca^{2+}]_i$ response compared to ATP with a mean amplitude of 0.7 ± 0.04 ($p = 0.01$; Fig. 4B). The application of adenosine (100 μM) had no effect. The application of 100 μM ATP in the absence of extracellular Ca^{2+} caused the most potent activation of purinergic receptors, significantly higher compared to BzATP ($p = 0.001$) and α,β-meATP ($p = 0.01$), but not to ATP ($p = 0.4$). ATP at low Ca^{2+} induced a $[Ca^{2+}]_i$ increase of 1.87 ± 0.49 in all 4 tested cells.

Increases in $[Ca^{2+}]_i$ induced by α,β-meATP were significantly (by 98 ± 0.4%) inhibited by pre-incubation with PPADS in all 4 cells tested (Fig. 4C). Neither $P2X_1$-selective antagonist NF279 (1 μM) nor $P2X_7$-selective antagonist KN-62 (1 μM) affected BzATP-induced $[Ca^{2+}]_i$ increase ($p = 0.7$, $n = 6$). Another antagonist, MRS2179, selective for $P2Y_1$ receptors also did not affect the ATP-induced Ca^{2+} responses ($p = 0.28$, $n = 4$).

The number of mBMSCs responsive to ATP increased (86%) when compared with bBMSCs (62%). mBMSCs were also sensitive to other agonists of purinergic receptors. Unlike mADSCs, where ATP was the most potent activator of purinoceptors, in mBMSCs the highest $[Ca^{2+}]_i$

responses were induced by BzATP. The amplitude of 20 μM BzATP-induced $[Ca^{2+}]_i$ increase was 1.69 ± 0.14, n = 15, significantly higher compared to 100 μM ATP (0.94 ± 0.08, n = 25, p = 0.00005) and to 100 μM α,β-meATP (0.64 ± 0.16. n = 6, p = 0.0003; Fig. 4B). Application of PPADS, a non-selective antagonist of P2X and $P2Y_{2,4}$ receptors, had no effect (p = 0.94, n = 7). KN-62 (1 μM), a selective $P2X_7$ antagonist, completely blocked BzATP-induced $[Ca^{2+}]_i$ increase in all cells tested (p = 0.01, n = 4) (Fig. 4D). Expression of $P2X_7R$ was also confirmed by immunocytochemical staining (Fig. 4E).

3.6. Vasopressin and oxytocin receptors

Application of 100 nM the neuropeptide vasopressin (AVP) increased $[Ca^{2+}]_i$ in 75% of tested bADSCs (n = 12) and all bBMSCs (n = 19) with a mean amplitude of 1.97 ± 0.3 and 1.36 ± 0.1, respectively (Table 1). In order to test the specificity of AVP action, we used a selective AVP-V_1 receptor antagonist, [deamino-Pen1, O-Me-Tyr2, Arg8]-vasopressin at 1 μM. Pre-incubation of cells with AVP-V_1 antagonist completely blocked the AVP (100 nM)-induced $[Ca^{2+}]_i$ response in all bADSCs and in 44% of bBMSCs. In the remaining 56% of bBMSCs, it suppressed the AVP (100 nM)-induced $[Ca^{2+}]_i$ response by 40 ± 4.8%, n = 4 (p = 0.036; Fig. 5A). On the other hand, neither bADSCs nor bBMSCs responded to another neuropeptide, oxytocin (OT), applied at concentrations of 100 nM or 1000 nM.

Unlike cells in basal conditions, which were sensitive to AVP but not to OT, mADSCs and mBMSCs were sensitive to both OT and AVP. OT at 1000 nM induced an increase in $[Ca^{2+}]_i$ in 87% of the mADSCs and 73% of mBMSCs tested (Table 1). This response did not desensitize during several sequential applications of OT (Fig. 5D, F) and was concentration-dependent (Fig. 5B). The mean amplitude of the $[Ca^{2+}]_i$ response to various OT concentrations in mADSCs ranged, respectively, from 0.23 ± 0.03, n = 4 for 10 nM, 0.95 ± 0.3, n = 4 for 500 nM and 1.22 ± 0.19, n = 13, for 1000 nM (Fig. 5B). The amplitudes of the $[Ca^{2+}]_i$ increase in mBMSCs were: 10 nM OT elicited a $[Ca^{2+}]_i$ rise of 0.32 ± 0.07, n = 9; 100 nM OT, 0.18 ± 0.04, n = 4; 500 nM OT, 0.59 ± 0.14, n = 6; and 1000 nM OT, 1.02 ± 0.18, n = 8 (Fig. 5B). Incubation with 1 μM $d(CH_2)_5OVT$, an OT receptor antagonist, completely blocked the OT-induced $[Ca^{2+}]_i$ rise in both mADSCs (n = 4, Fig. 5H) and mBMSCs (n = 4, Fig. 5J). Immunocytochemical staining with an oxytocin antibody confirmed the presence of OT in the cultured mADSCs (Fig. 5L) and mBMSCs (Fig. 5N).

Application of AVP evoked reproducible (Fig. 5E, G) and dose-dependent (Fig. 4C) increases in $[Ca^{2+}]_i$ in 94% of the mADSCs and all mBMSCs tested (Table 1). The mean amplitude of $[Ca^{2+}]_i$ increase in mADSCs was 2.31 ± 0.23, n = 5 at 10 nM AVP; 2.17 ± 0.18, n = 17 at 100 nM AVP; 1.26 ± 0.31, n = 4 at 500 nM AVP and 1.16 ± 0.25, n = 6 for 1000 nM AVP (Fig. 5C). In mBMSCs the amplitude of $[Ca^{2+}]_i$ increases was 1.03 ± 0.14, n = 7 in response to 100 nM AVP; 0.91 ± 0.17, n = 6 in response to 500 nM AVP and 0.63 ± 0.07, n = 7 in response to 1000 nM AVP (Fig. 5C). Unlike OT, which in high concentrations caused a higher $[Ca^{2+}]_i$ increases, AVP when applied at a high dose inhibited AVP receptors. Application of V_1 selective antagonist [deamino-Pen^1, O-Me-Tyr^2, Arg^8]-vasopressin completely blocked AVP-induced $[Ca^{2+}]_i$ increases in all 9 mADSCs tested (Fig. 5I) and significantly inhibited by 95 ± 0.7% in all 5 tested mBMSCs (p = 0.0005, Fig. 5K), confirming that functional AVP-V_1 receptors are present in all mADSCs and mBMSCs. Immunocytochemical staining with a vasopressin antibody revealed the presence of AVP both in mADSCs (Fig. 5M) and mBMSCs (Fig. 5O).

3.7. Membrane properties of ADSCs and BMSCs

The passive membrane properties of bADSCs and bBMSCs are listed in Table 2. Most notable, mADSCs and mBMSCs exhibited a significant hyperpolarizing shift of resting membrane potential. In the voltage-clamp settings bADSCs and bBMSCs displayed, in response to de- and hyperpolarizing test pulses, symmetrical currents that decayed during the voltage steps. These currents had a linear current–voltage relationship with E_{rev} at −33.2 ± 4.9 mV (n = 26) for bADSCs and −57.1 ± 8.7 mV (n = 23) for bBMSCs (Fig. 6A, B). An increase in extracellular K^+ from 3 mM to 30 mM caused a positive shift in reversal potential in bADSCs by 14 ± 6.7 mV (n = 6) and in bBMSCs by 28 ± 3.1, mV (n = 7). In medium modified cells, voltage pulses similarly evoked symmetric currents, which however were mainly time-independent. The voltage–current relation for these currents was linear with reversal potential at −71.8 + 1.4 mV (n = 30) for p ADSCs and −71.5 + 1.5 mV (n = 22) for mBMSCs (Fig. 6C, D). Both, bADSCs and bBMSCs expressed vimentin, the marker of progenitor cells (Fig. 6E).

4. Discussion

In this study, we investigated Ca^{2+} signaling and electrophysiological properties of rat stromal cells obtained from adipose tissue and bone marrow. We analyzed the changes of functional properties under the same environmental conditions upon medium modification that were previously reported to elicit changes in ADSCs (Willingham and Pastan, 1975). We demonstrated that after medium modification, both ADSCs and BMSCs undergo a significant change in their membrane properties and in the expression of channels and receptors associated with generation of Ca^{2+} signals (Fig. 7). The resting $[Ca^{2+}]_i$ level in mBMSCs significantly decreased after pre-differentiation and became almost the same as in ADSCs. The resting $[Ca^{2+}]_i$ level in ADSCs remained unchanged after medium modification.

4.1. Voltage-gated Ca^{2+} channels

VGCCs were found in several preparations of stem cells. High voltage activated L-type Ca^{2+} channels were shown to enhance proliferation and osteogenic differentiation in rat BMSCs (Wen et al., 2012). Small dihydropyridine-sensitive currents were recorded in minor subpopulations of undifferentiated BMSCs from humans and rats (Kawano et al., 2002; Heubach et al., 2004; Li et al., 2005, 2006). We were not able to detect any VGCCs-mediated Ca^{2+} entry in BMSCs in basal conditions. This could be explained by differences in the techniques and culture conditions. However, after medium modification, almost half of the cells (42%) were sensitive to depolarization with 50 mM K^+. In our experiments, nicardipine completely blocked high K^+-induced $[Ca^{2+}]_i$ responses confirming the functional expression of L-type Ca^{2+} channels both in mADSCs and mBMSCs (Fig. 2). In mBMSCs, ω-conotoxin MVIIC, a selective P/Q-type Ca^{2+} channel blocker, significantly inhibited K^+-induced $[Ca^{2+}]_i$ increase, suggesting the additional activation of P/Q-type channels. To our knowledge, this is the first report showing the functional P/Q-type Ca^{2+} channels in rats BMSCs. We were not able to identify N-type Ca^{2+} channels in BMSCs, either functionally or at the protein expression level. In contrast, several studies demonstrated the (mRNA and protein) expression of CACNA 1 C (L-type) and CACNA 1 G (T-type) in ADSCs in basal and medium-modified conditions (Safford et al., 2004; Bai et al., 2007; Jang et al., 2010). Immunocytochemically, the presence of both the CACNA 1 C subunit of L-type Ca^{2+} channels and the CACNA 1 A subunit of P/Q-type Ca^{2+} channels was detected in mADSCs and mBMSCs.

In summary, depolarization of bBMSCs and bADSCs did not produce $[Ca^{2+}]_i$ transients, likely indicating the absence of functional VGCCs. Conversely, almost half of the population of mBMSCs (42%) and mADSCs (46%) generated a $[Ca^{2+}]_i$ increase in response to depolarization. mBMSCs and mADSCs expressed functional L-type Ca^{2+} channels and a small population of mADSCs (but not mBMSCs) expressed P/Q-type Ca^{2+} channels as well.

4.2. Spontaneous oscillations and intracellular Ca^{2+} stores

Spontaneous $[Ca^{2+}]_i$ oscillations contribute to many cellular processes, such as secretion, fertilization, etc. (Berridge et al., 2000; Ye, 2010).

In our study, (similarly to that of Ichikawa et al. (Ichikawa and Gemba, 2009)), we did not observe spontaneous oscillations in BMSCs in basal conditions, although 29% of mBMSCs exhibited spontaneous $[Ca^{2+}]_i$ activity. Exposure to non-selective VGCC antagonists, Cd^{2+} and Ni^{2+}, significantly inhibited the amplitude of spontaneous $[Ca^{2+}]_i$ increases, but did not block them completely, suggesting the role for intracellular

A

	bADSCs	mADSCs	bBMSCs	mBMSCs
RyR1	++	++	++	++
RyR2	++	+	-	-
RyR3	++	++	+	++

" - " - negative immunostaining
" + " - faint positive immunostaining / few cells express the marker
"++" - positive immunostaining / majority cells express the marker

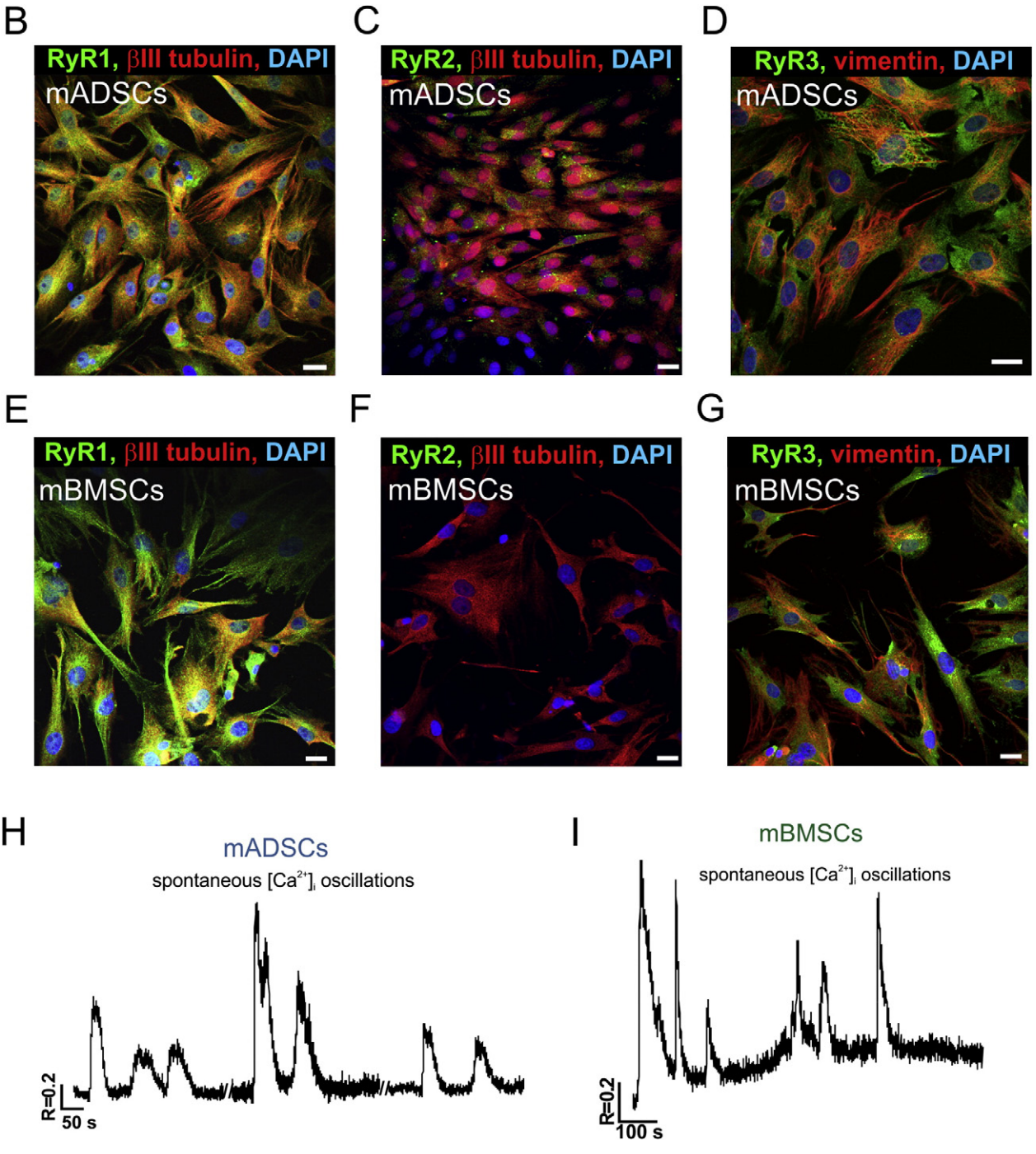

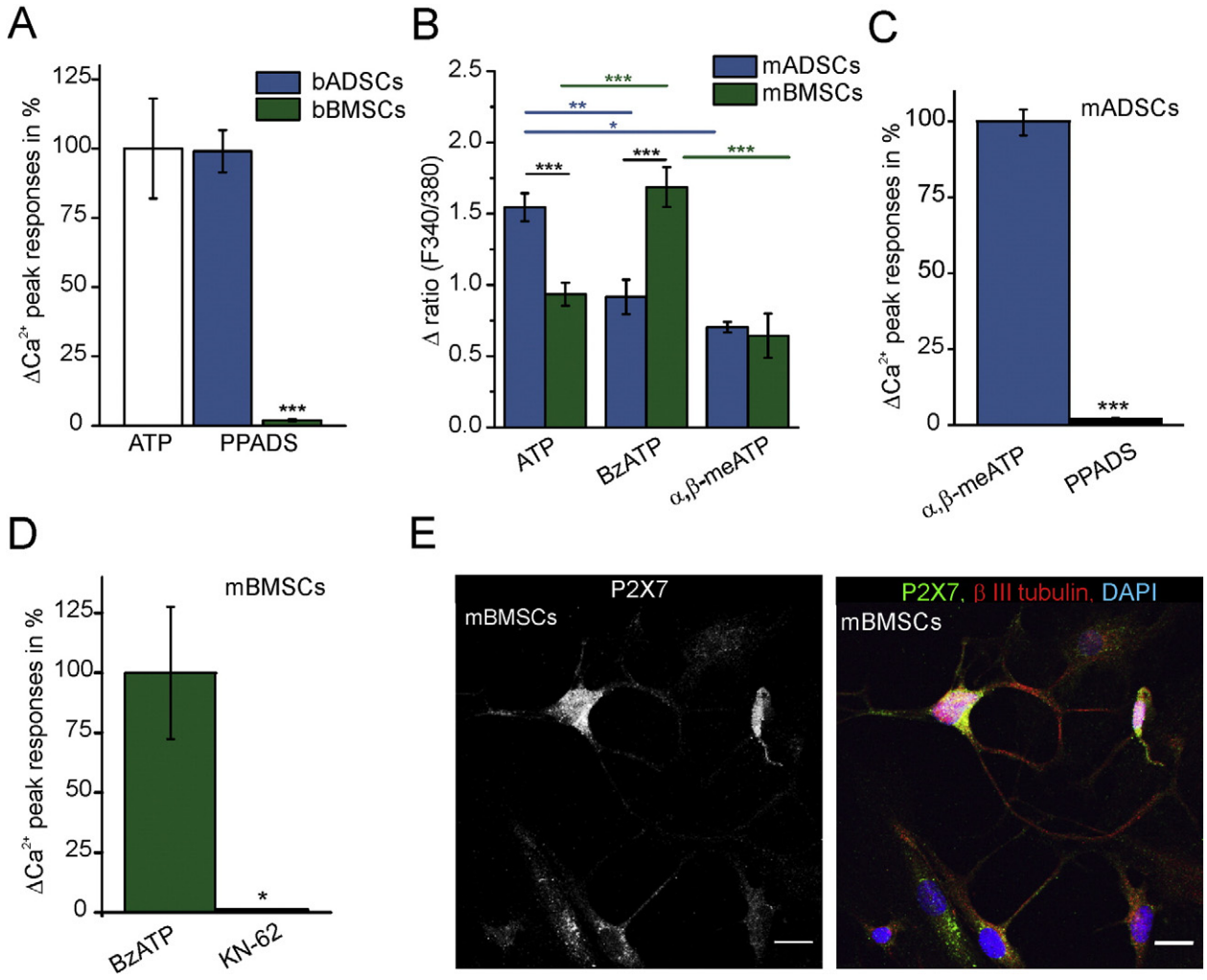

Fig. 4. Purinergic responses in ADSCs and BMSCs under basal and medium modified conditions. A. Bar diagram showing the percentage of the mean peak amplitude of $[Ca^{2+}]_i$ increase before (ATP control) and after incubation with the 10 μM PPADS in bBMSCs and bADSCs (***$p = 0.0004$, $n = 5$). Control ATP-induced $[Ca^{2+}]_i$ increase was taken as 100%. B. Bar diagrams showing the evoked mean amplitude of $[Ca^{2+}]_i$ increase (fluorescence ratio units) in response to various purinergic receptor agonists in mADSCs (blue) and mBMSCs (green). Data are mean ± S.E.M. The cells were exposed to 100 μM ATP, 20 μM BzATP and 100 μM α,β-meATP. The significance between mADSCs and mBMSCs is shown by asterisks in black; between various agonists among mADSCs in blue; and between various agonists among mBMSCs in green. C. Bar diagram showing the percentage of mean peak amplitude of the $[Ca^{2+}]_i$ increase before (α,β-meATP control) and after incubation with the 10 μM PPADS in mADSCs. Control α,β-meATP-induced $[Ca^{2+}]_i$ increase was taken as 100%. D. mBMSCs. Bar diagram showing the percentage mean peak amplitude of the $[Ca^{2+}]_i$ increase before (BzATP as control) and after incubation with the $P2X_7$ receptor blocker KN-62. Control BzATP-induced $[Ca^{2+}]_i$ increase was taken as 100%. *$p < 0.05$; **$p < 0.01$; ***$p < 0.001$. E. Confocal image showing mBMSCs co-stained for $P2X_7$ receptor (green) and βIII tubulin (red). Cell nuclei are visualized with DAPI staining. Single P2X7 staining is shown on the left panel. Scale bars = 20 μm.

Ca^{2+} stores and VGCC; these findings are in accordance with previous reports (Kawano et al., 2002, 2003). Spontaneous $[Ca^{2+}]_i$ oscillations were also observed in a subpopulation of human ADSCs; although the numbers of responding cells differed remarkably from 2 to 5% (Kotova et al., 2014) to 70% (Sauer et al., 2011). In our case, in rat ADSCs spontaneous $[Ca^{2+}]_i$ oscillations were observed only in a small subpopulation (12% of bADSCs and 13% of mADSCs). These spontaneous $[Ca^{2+}]_i$ dynamics were not inhibited after removal of extracellular Ca^{2+}, suggesting that intracellular $[Ca^{2+}]_i$ stores underlie these oscillations. In addition, mADSCs were sensitive to the application of 2 μM ryanodine and 10 μM CPA, suggesting that mADSCs possess functional ER Ca^{2+} stores and ryanodine receptors.

4.3. Purinergic receptors

Purinergic signaling plays an important role during stem cell development, influencing proliferation and determining cell fate, although the effects of agonists depend on the receptor subtype (Forostyak et al., 2013). For example ATP, acting through P2X receptors, induces the proliferation of human hematopoietic stem cells (Glaser et al., 2012). BMSCs at early passages (P0–P5) spontaneously release ATP and inhibit cell proliferation. Inhibition of $P2Y_1$ receptors led to increased proliferation (Coppi et al., 2007); the same $P2Y_1$ receptors in human BMSCs also contributed to $InsP_3$-induced spontaneous $[Ca^{2+}]_i$ oscillations (Kawano et al., 2006). Here we also investigated the

Fig. 3. Spontaneous $[Ca^{2+}]_i$ transients and immunocytochemical analysis for ryanodine receptors in ADSCs and BMSCs. A. Table showing the expression of ryanodine receptors 1–3 in basal and medium-modified ADSCs and BMSCs. Confocal images showing the co-localization of immunocytochemical staining for cytoskeletal marker βIII tubulin (red) and ryanodine receptor-1 (RyR1, green) in mADSCs (B) and mBMSCs (E). C, and F show co-localization of βIII tubulin (red) and ryanodine receptor-2 (RyR2, green) in mADSCs (C) and mBMSCs (F). The co-localization of the markers for vimentin proliferation (red) and ryanodine receptor-3 (RyR3, green) in mADSCs and mBMSCs is shown in D and G, respectively. Cell nuclei were visualized with DAPI staining. Scale bars = 20 μm. H, I. The representative traces showing spontaneous $[Ca^{2+}]_i$ oscillations observed in mADSCs (H) and mBMSCs (I).

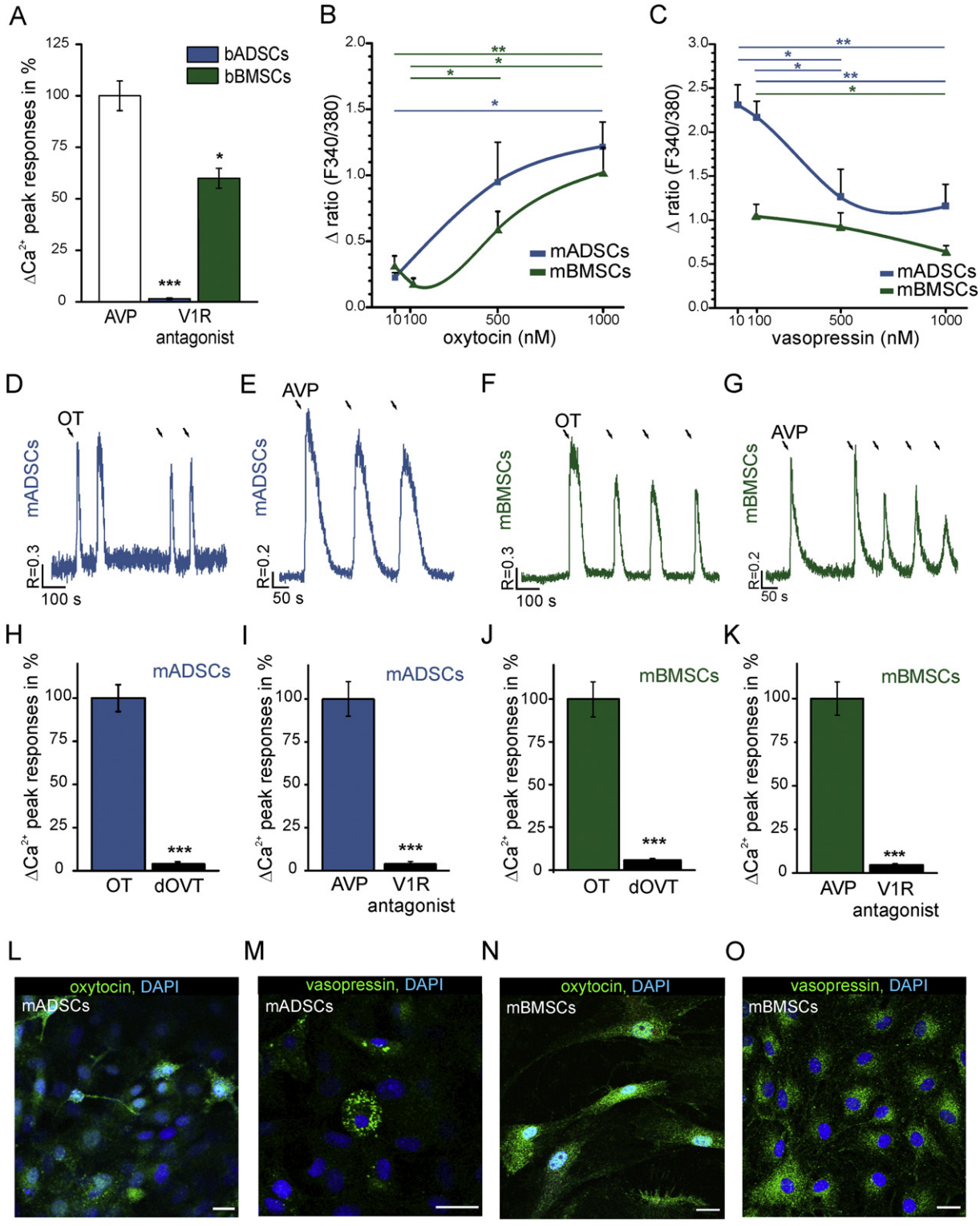

Fig. 5. Oxytocin and vasopressin responses in ADSCs and BMSCs in basal and medium modified conditions. A. Bar diagram showing the percentage of the mean peak amplitude of $[Ca^{2+}]_i$ increase before (AVP control) and after incubation with the 1 μM AVP-V_1R antagonist, (d(CH_2)$^1_5$, Tyr(Me)^2, Arg^8)-vasopressin in bBMSCs and bADSCs (*p = 0.036, n = 4). Control AVP-induced $[Ca^{2+}]_i$ increase was taken as 100%. B. Dose-dependent $[Ca^{2+}]_i$ increase in response to application of increasing concentrations OT in mADSCs (blue curve) and mBMSCs (green curve). Similarly, C. Dose-dependent $[Ca^{2+}]_i$ increase in response to the application of increasing concentrations of AVP in mADSCs (blue curve) and mBMSCs (green curve). The significance between various agonists among mADSCs and mBMSCs is shown by asterisks in blue and green, respectively. Data are mean ± S.E.M. *p < 0.05; **p < 0.01; ***p < 0.001. D–G. Representative traces of an individual mADSCs (D, E) or mBMSCs (F, G) subjected to successive 10 s applications 100 nM OT (D, F) or 100 nM AVP (E, G). H, J. Bar diagrams representing the peak amplitude $[Ca^{2+}]_i$ (control percentage) response induced by 100 nM OT and a significant inhibition by the presence of OT-antagonist, 1 μM dOVT in mADSCs (H) and mBMSCs (J). I, K. Bar diagrams representing the peak amplitude $[Ca^{2+}]_i$ (control percentage) response induced by 100 nM AVP and a significant inhibition by the presence of 1 μM AVP-V_1R antagonist, in mADSCs (I) and mBMSCs (K). K–N. Immunohistochemical detection of OT and AVP in mADSCs and in mBMSCs. Confocal images showing mADSCs stained for OT (L), AVP (M) and nuclear DAPI staining. Similarly, confocal images showing mBMSCs stained for OT (N), AVP (O) and nuclear DAPI staining. Scale bars = 20 μm.

Table 2
The passive membrane properties of ADSCs and BMSCs in basal and medium modified conditions.

		ADSCs		BMSCs	
		Basal	Modified	Basal	Modified
V_{rest}	[mV]	−33.9 ± 2.0	−77.5 ± 1.5***	−49.7 ± 3.6	−77.9 ± 1.6***
E_{rev}	[mV]	−33.2 ± 4.9	−71.8 ± 1.4***	−57.1 ± 8.7	−71.5 ± 1.7
C_m	[pF]	59.2 ± 12.5	59.6 ± 4.4	66.1 ± 9.3	54.0 ± 4.1
IR	[MΩ]	131.5 ± 14.5	53.3 ± 5.4	140.5 ± 29.6	56.7 ± 5.1**
n		26	30	23	22

Asterisks indicate significant vs cells in basal conditions within the same cell line (*p ≥ 0.05; **p ≥ 0.01; ***p ≥ 0.001).

presence of $P2Y_1$ receptors in mADSCs and mBMSCs, but were unable to dissect P2Y receptors in mBMSCs, which could be explained by the different species from which the cells were obtained. In mADSCs, ATP-induced $[Ca^{2+}]_i$ responses were observed after the removal of Ca^{2+} from an external medium and these responses were not blocked by MRS2179 (a selective $P2Y_1$ antagonist) suggesting that mADSCs express P2Y receptors distinct from $P2Y_1$. We found that 62% of bBMSCs and 90% of bADSCs were sensitive to ATP, but not to other neurotransmitters, possibly reflecting the fact that purinergic receptors are one of the first neurotransmitter receptors expressed in development (Glaser et al., 2012). The number of cells sensitive to ATP increased to 86% in mBMSCs and 100% in mADSCs). Neither ADSCs nor BMSCs were sensitive to adenosine, thus excluding the role of P1 adenosine receptors.

The broad agonist BzATP can activate all P2X receptors. However, $P2X_1$ and $P2X_7$ receptors exhibit sensitivity an order greater than to ATP (Syed and Kennedy, 2012). The order of potency of P2 receptor agonists in mBMSCs was as follows: BzATP > ATP > α,β-meATP. Selective $P2X_7$ antagonist KN-62 effectively blocked the BzATP-induced $[Ca^{2+}]_i$ increase in mBMSCs (but not in bBMSCs), confirming the activation of $P2X_7$ receptors. The mADSCs were more sensitive to ATP (the potency order ATP > BzATP > α,β-meATP), and KN-62 had no effect, suggesting the absence of functional $P2X_7$ receptors. Instead, an α,β-meATP-induced $[Ca^{2+}]_i$ increase in mADSCs was effectively blocked by PPADS, a non-selective blocker of P2X receptors. Since PPADS is ineffective on $P2X_4$ and KN-62 had no effect, we suggest that mADSCs express P2X receptors, but not $P2X_4$ or $P2X_7$. The presence of $P2X_7$ receptors in mBMSCs, but not in mADSCs, was also confirmed by immunocytochemical studies (Fig. 4). We conclude that although both mADSCs and mBMSCs express P2 receptors, the BMSCs expressed only $P2X_7$ receptors, ADSCs expressed both P2X (but not $P2X_7$) and P2Y (but not $P2Y_1$) receptors.

4.4. Oxytocin and vasopressin

OT and AVP control a wide range of functions in the central as well as in the peripheral nervous systems (Dayanithi et al., 2000, 2008, 2012; Hussy et al., 2001; Ueta et al., 2008; Suzuki et al., 2009; Fujihara et al., 2009; Todoroki et al., 2010; Viero et al., 2010; Moriya et al., 2012, 2015). The primary cultures of neonatal rat cardiomyocytes express OT receptors (Florian et al., 2010). Recently OT has become a subject of increased attention due to its protective and metabolic effects on rats (male Sprague Dawley) BMSCs. Stimulated by pretreatment with OT, BMSCs have been shown to reduce apoptosis, and increase cellular proliferation and glucose uptake (Noiseux et al., 2012). OT was also shown to control ADSC differentiation (Elabd et al., 2008; Jafarzadeh et al., 2014) and proliferation (Jafarzadeh et al., 2014). bADSCs and bBMSCs in our study were not sensitive to OT, although most mBMSCs (73%) and mADSCs (87%) responded to OT by an increase in $[Ca^{2+}]_i$. These responses were reproducible and dose-dependent (Fig. 5). These findings are in accordance with previous reports confirming the role of OT during the differentiation of both human BMSCs and ADSCs (Elabd et al., 2008; Jafarzadeh et al., 2014).

There are few reports on the role of AVP in the life of stem cells, although it has been shown that AVP contributes to myogenic differentiation (Scicchitano et al., 2005) and cardiac development by inducing the differentiation of atrial and ventricular precursor cells (Gassanov et al., 2007). To our knowledge there are no reports on the role of AVP in ADSCs and BMSCs. We observed that both bBMSCs and mBMSCs were sensitive to AVP. Similarly, the majority of bADSCs (75%) and mADSCs (94%), responded to AVP by an increase in $[Ca^{2+}]_i$. This increase was dose-dependent and high doses of AVP (1000 nM and 500 nM) induced a significantly lower $[Ca^{2+}]_i$ rise compared to low doses (10 nM and 100 nM), suggesting the inhibitory role of higher concentrations of AVP (Fig. 5). AVP-induced $[Ca^{2+}]_i$ increases were mediated by the V_1-type AVP receptor. The expression of V_{1a}-type of AVP receptors was also demonstrated in human ADSCs (Tran et al., 2015). Previously, it was reported that AVP promotes the proliferation of rat cardiac fibroblast through V_1 receptors (Yang et al., 2003). Tran et al. have reported that AVP-V_{1a} receptor gene expression in hASCs and AVP inhibits adipogenesis in this stem cell type (Tran et al., 2015).

4.5. Glutamate

We found that neither bBMSCs nor mBMSCs were sensitive to the application of glutamate. In contrast, a subpopulation (27%) of mADSCs were sensitive to glutamate, but not to NMDA, suggesting the activation of glutamate receptors distinct from NMDA receptors. A glutamate-induced $[Ca^{2+}]_i$ increase was observed previously in a very small population of ADSCs (3.6%) (Kotova et al., 2014).

4.6. Ion channels and membrane properties

mADSCs and mBMSCs displayed a remarkable shift in the nature of their membrane conductances. In cells cultured in basal conditions, the predominant passive conductance reversed at ~−40 to −50 mV; that is, at levels much more positive than the E_K (calculated at −84 mV) for given experimental conditions. Furthermore, a 10-fold increase in extracellular K^+ produced a relatively minor shift in E_{rev} (14 mV and 28 mV for bAMSCs and bBMSCs respectively), which was much less than the theoretically predicted shift of 59 mV for K^+ selective conductance. This indicates the non-selective nature of the resting membrane conductance, which may be mediated by the mixture of non-selective, K^+ and possibly even anion channels. In mADSCs and mBMSCs, in contrast, the reversal potential for passive currents was very close to the E_K, indicating predominance of K^+ conductance. This shift from non-selective conductance to K^+ conductance explains well the much more hyperpolarized resting potential of mADSCs and mBMSCs.

Different types of channels have been reported in adherent, fibroblastic stem/progenitor cells of different origins and in different culture conditions from both humans and rats (Forostyak et al., 2016). For example, undifferentiated BMSCs were shown to display large K^+ conductance (Zhu et al., 2015), mediated by inward rectifying and delayed rectifying K^+ channels as well as by Ca^{2+}−activated K^+ currents (Deng et al., 2006). In contrast, the membrane conductance of adipocytes was mainly mediated by non-selective cationic channels and Cl^- channels (Bentley et al., 2014), although two-pore domain K^+ channels K3 (KCNK3, TASK-1) were described in human adipocytes (Shinoda et al., 2015). Precise identifications of ion channel types expressed in tissue specific stem/progenitor cells at various differentiated stages require further investigation.

5. Conclusions

Together, as briefly summarized in Fig. 7, our results suggest that the Ca^{2+} signaling, ion channel and ionotropic receptor expression profile of adult tissue-specific stem/progenitor cells depends not only on the culture conditions but also on the source from which the cells were

isolated. The fate and functional properties of differentiated cells are driven by intrinsic mechanisms, which are independent of the culture protocol. Identifying their Ca^{2+} signaling, ion channel and ionotropic receptor expression profile as a function of external changes in their environment is essential to better utilize these cells in tissue engineering and regenerative medicine.

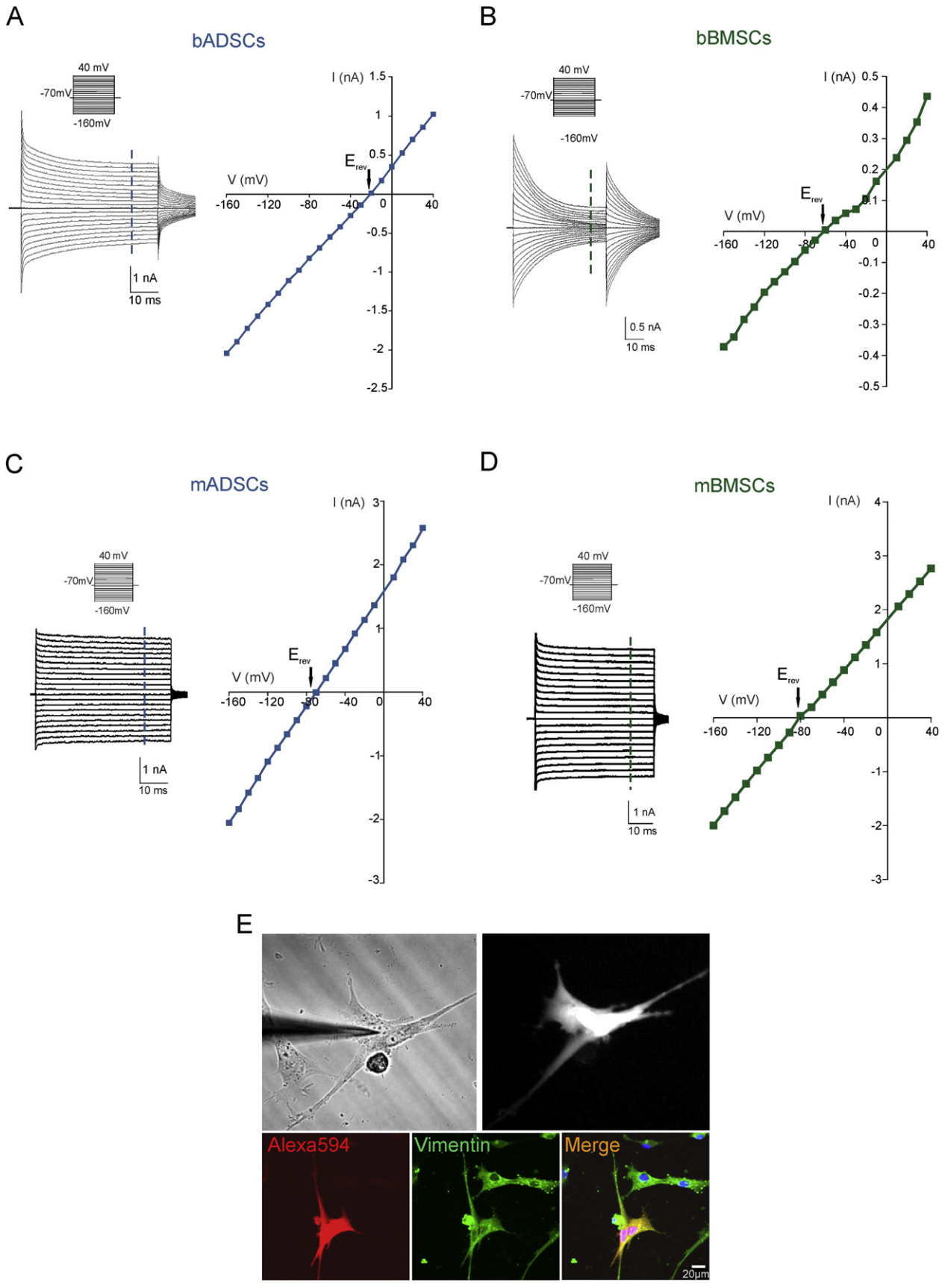

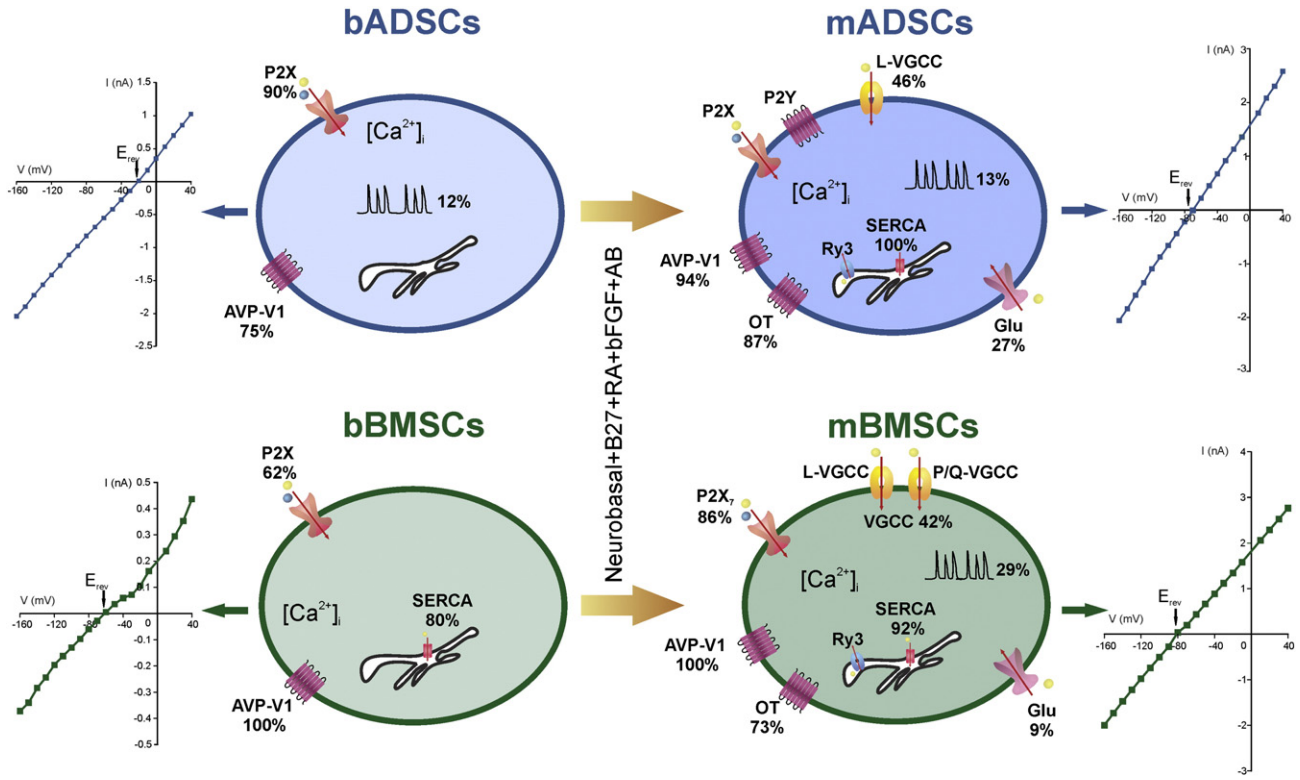

Fig. 7. Schematic drawing showing the change in functional expression of Ca^{2+} channels and receptors linked to Ca^{2+} signaling in ADSCs and BMSCs following medium modification. Both ADSCs and BMSCs were subjected to the same culture conditions. The function of voltage-gated Ca^{2+} channels, as well as ryanodine, purinergic, glutamate, vasopressin and oxytocin receptors were analyzed and compared in ADSCs and BMSCs before and after medium modification.

Supplementary data to this article can be found online at http://dx.doi.org/10.1016/j.scr.2016.03.010.

Authors' contributions

O.F. contributed to prepare experimental design, performed Ca^{2+} measurements, helped with data and statistical analysis, immunocytochemistry, confocal imaging, and contributed in manuscript writing.

O.B. performed patch-clamp experiments, helped with electrophysiological data analysis and related statistics, and contributed in manuscript writing on electrophysiological data.

M.A. supervised patch-clamp experiments, helped with electrophysiological data analysis and related statistics, and contributed in manuscript writing on electrophysiological data.

S.F. helped with preparing cell culture and confocal imaging experiments and imaging analysis.

E.S. participated in experimental design, organized logistics, and participated in manuscript writing.

A.V. provided experimental design, helped with electrophysiological data analysis and related statistics, and interpreting the data, and contributed in manuscript writing and editing.

G.D. provided concept and experimental design, project management, supervised the experiments, checked the data and statistical analysis and interpretation, and wrote the manuscript.

Disclosure of potential conflicts of interest

The authors declare that they have no conflicts of interest.

Acknowledgments

This work was supported by the grants GACR 14-34077S, GACR P304/11/2373, GACR P304/12/G069 and GACR 10504P from the Grant Agency of the Czech Republic. This publication is partly a result of the "Advanced Bioimaging of Living Tissues" project, registration number #CZ.2.16/3.1.00/21527, which was financed from the budget of the European Regional Development Fund and public budgets of the Czech Republic through the Operational Programme Prague — Competitiveness. AV was supported by the Wellcome Trust, by the Alzheimer's research foundation (UK) and by the grant (agreement from August 27, 2013 no. 02.B.49.21.0003) between The Ministry of Education and Science of the Russian Federation and Lobachevsky State University of Nizhny Novgorod, by the grant of the Russian Scientific Foundation no.14-15-00633 and by the Ministry of Education of the Russian Federation, unique identity number RFMEFI57814X0079. Govindan Dayanithi belongs to the "Centre National de la Recherche Scientifique—The French Ministry of Research and Higher Education-Paris", France. We thank David Arboleda and Lenka Baranovicova for their participation in preliminary experiments. We are grateful to Kip Allan Bauersfeld, IEM ASCR, for critical reading and helpful comments on the manuscript.

References

Al-Nbaheen, M., Vishnubalaji, R., Ali, D., et al., 2013. Human stromal (mesenchymal) stem cells from bone marrow, adipose tissue and skin exhibit differences in molecular phenotype and differentiation potential. Stem Cell Rev. 9, 32–43.

Fig. 6. Ion current profiles obtained from basal and medium-modified ADSCs and BMSCs. The current families were obtained in response to hyper- and depolarizing test pulses from the holding potential, −70 mV (see the insets). A, B. current traces and current to voltage relations obtained from bADSCs and bBMSCs. The reversal potentials are indicated by arrows; the E_{rev} are −33.2 + 4.9 mV (n = 26) for bADSCs and −57.1 + 8.7 mV (n = 23) for bBMSCs. C, D. Current traces and current to voltage relations obtained from mADSCs and mBMSCs. The reversal potentials are indicated by arrows; the E_{rev} are −71.8 + 1.4 mV (n = 30) for mADSCs and −71.5 + 1.7 mV (n = 22) for mBMSCs. E. An image of Alexa594-loaded an adipose-derived stromal cell in basal conditions, taken by a digital camera immediately after patch-clamp recording and the same cell immunostained with antibody against vimentin. The overlay image shows the co-localization of vimentin with Alexa594.

Anderova, M., Kubinova, S., Jelitai, M., et al., 2006. Transplantation of embryonic neuroectodermal progenitor cells into the site of a photochemical lesion: Immunohistochemical and electrophysiological analysis. J. Neurobiol. 66 (10), 1084–1100.
Arboleda, D., Forostyak, S., Jendelova, P., et al., 2011. Transplantation of predifferentiated adipose-derived stromal cells for the treatment of spinal cord injury. Cell. Mol. Neurobiol. 31, 1113–1122.
Bai, X., Ma, J., Pan, Z., et al., 2007. Electrophysiological properties of human adipose tissue-derived stem cells. Am. J. Physiol. Cell. Physiol. 293, C1539–C1550.
Barry, P.H., 1994. JPCalc, a software package for calculating liquid junction potential corrections in patch-clamp, intracellular, epithelial and bilayer measurements and for correcting junction potential measurements. J. Neurosci. Methods 51, 107–116.
Bentley, D.C., Pulbutr, P., Chan, S., et al., 2014. Etiology of the membrane potential of rat white fat adipocytes. Am. J. Physiol. Endocrinol. Metab. 307, E161–E175.
Berridge, M.J., Lipp, P., Bootman, M.D., 2000. The versatility and universality of calcium signalling. Nat. Rev. Mol. Cell Biol. 1, 11–21.
Choudhery, M.S., Badowski, M., Muise, A., et al., 2013. Comparison of human mesenchymal stem cells derived from adipose and cord tissue. Cytotherapy 15, 330–343.
Cocks, G., Romanyuk, N., Amemori, T., et al., 2013. Conditionally immortalized stem cell lines from human spinal cord retain regional identity and generate functional v2a interneurons and motorneurons. Stem Cell Res. Ther. 4, 69.
Coppi, E., Pugliese, A.M., Urbani, S., et al., 2007. ATP modulates cell proliferation and elicits two different electrophysiological responses in human mesenchymal stem cells. Stem Cells 25, 1840–1849.
Dayanithi, G., Forostyak, O., Ueta, Y., et al., 2012. Segregation of calcium signalling mechanisms in magnocellular neurones and terminals. Cell Calcium 51, 293–299.
Dayanithi, G., Mechaly, I., Viero, C., et al., 2006. Intracellular Ca2+ regulation in rat motoneurons during development. Cell Calcium 39, 237–246.
Dayanithi, G., Sabatier, N., Widmer, H., 2000. Intracellular calcium signalling in magnocellular neurones of the rat supraoptic nucleus: understanding the autoregulatory mechanisms. Exp. Physiol. 75S–84S 85 Spec No.
Dayanithi, G., Viero, C., Shibuya, I., 2008. The role of calcium in the action and release of vasopressin and oxytocin from CNS neurones/terminals to the heart. J. Physiol. Pharmacol. 59 (Suppl. 8), 7–26.
Dayanithi, G., Widmer, H., Richard, P., 1996. Vasopressin-induced intracellular Ca2+ increase in isolated rat supraoptic cells. J. Physiol. 490 (Pt 3), 713–727.
Deng, X.L., Sun, H.Y., Lau, C.P., et al., 2006. Properties of ion channels in rabbit mesenchymal stem cells from bone marrow. Biochem. Biophys. Res. Commun. 348, 301–309.
Elabd, C., Basillais, A., Beaupied, H., et al., 2008. Oxytocin controls differentiation of human mesenchymal stem cells and reverses osteoporosis. Stem Cells 26, 2399–2407.
Florian, M., Jankowski, M., Gutkowska, J., 2010. Oxytocin increases glucose uptake in neonatal rat cardiomyocytes. Endocrinology 151, 482–491.
Forostyak, O., Forostyak, S., Kortus, S., et al., 2016. Physiology of ca signalling in stem cells of different origins and differentiation stages. Cell Calcium http://dx.doi.org/10.1016/j.ceca.2016.02.001 (in Press).
Forostyak, S., Jendelova, P., Kapcalova, M., et al., 2011. Mesenchymal stromal cells prolong the lifespan in a rat model of amyotrophic lateral sclerosis. Cytotherapy 13, 1036–1046.
Forostyak, O., Romanyuk, N., Verkhratsky, A., et al., 2013. Plasticity of calcium signaling cascades in human embryonic stem cell-derived neural precursors. Stem Cells Dev. 22, 1506–1521.
Fox, L.E., Shen, J., Ma, K., et al., 2010. Membrane properties of neuron-like cells generated from adult human bone-marrow-derived mesenchymal stem cells. Stem Cells Dev. 19, 1831–1841.
Fujihara, H., Ueta, Y., Suzuki, H., et al., 2009. Robust up-regulation of nuclear red fluorescent-tagged fos marks neuronal activation in green fluorescent vasopressin neurons after osmotic stimulation in a double transgenic rat. Endocrinology 150, 5633–5638.
Gassanov, N., Jankowski, M., Danalache, B., et al., 2007. Arginine vasopressin-mediated cardiac differentiation: insights into the role of its receptors and nitric oxide signaling. J. Biol. Chem. 282, 11255–11265.
Glaser, T., Cappellari, A.R., Pillat, M.M., et al., 2012. Perspectives of purinergic signaling in stem cell differentiation and tissue regeneration. Purinergic Signal 8, 523–537.
Heubach, J.F., Graf, E.M., Leutheuser, J., et al., 2004. Electrophysiological properties of human mesenchymal stem cells. J. Physiol. 554, 659–672.
Hussy, N., Bres, V., Rochette, M., et al., 2001. Osmoregulation of vasopressin secretion via activation of neurohypophysial nerve terminals glycine receptors by glial taurine. J. Neurosci. 21, 7110–7116.
Ichikawa, J., Gemba, H., 2009. Cell density-dependent changes in intracellular Ca2+ mobilization via the p2y2 receptor in rat bone marrow stromal cells. J. Cell. Physiol. 219, 372–381.
Jafarzadeh, N., Javeri, A., Khaleghi, M., et al., 2014. Oxytocin improves proliferation and neural differentiation of adipose tissue-derived stem cells. Neurosci. Lett. 564, 105–110.
Jang, S., Cho, H.H., Cho, Y.B., et al., 2010. Functional neural differentiation of human adipose tissue-derived stem cells using bfgf and forskolin. BMC Cell Biol. 11, 25.
Kawano, S., Otsu, K., Kuruma, A., et al., 2006. Atp autocrine/paracrine signaling induces calcium oscillations and nfat activation in human mesenchymal stem cells. Cell Calcium 39, 313–324.
Kawano, S., Otsu, K., Shoji, S., et al., 2003. Ca(2+) oscillations regulated by Na(+)-Ca(2+) exchanger and plasma membrane Ca(2+) pump induce fluctuations of membrane currents and potentials in human mesenchymal stem cells. Cell Calcium 34, 145–156.
Kawano, S., Shoji, S., Ichinose, S., et al., 2002. Characterization of Ca(2+) signaling pathways in human mesenchymal stem cells. Cell Calcium 32, 165–174.
Kern, S., Eichler, H., Stoeve, J., et al., 2006. Comparative analysis of mesenchymal stem cells from bone marrow, umbilical cord blood, or adipose tissue. Stem Cells 24, 1294–1301.
Komori, Y., Tanaka, M., Kuba, M., et al., 2010. Ca(2+) homeostasis, Ca(2+) signalling and somatodendritic vasopressin release in adult rat supraoptic nucleus neurones. Cell Calcium 48, 324–332.
Kotova, P.D., Sysoeva, V.Y., Rogachevskaja, O.A., et al., 2014. Functional expression of adrenoreceptors in mesenchymal stromal cells derived from the human adipose tissue. Biochim. Biophys. Acta 1843, 1899–1908.
Lambert, R.C., Dayanithi, G., Moos, F.C., et al., 1994. A rise in the intracellular Ca2+ concentration of isolated rat supraoptic cells in response to oxytocin. J. Physiol. 478 (Pt 2), 275–287.
Lanner, J.T., Georgiou, D.K., Joshi, A.D., et al., 2010. Ryanodine receptors: structure, expression, molecular details, and function in calcium release. Cold Spring Harb. Perspect. Biol. 2, a003996.
Li, G.R., Deng, X.L., Sun, H., et al., 2006. Ion channels in mesenchymal stem cells from rat bone marrow. Stem Cells 24, 1519–1528.
Li, G.R., Sun, H., Deng, X., et al., 2005. Characterization of ionic currents in human mesenchymal stem cells from bone marrow. Stem Cells 23, 371–382.
Moriya, T., Kayano, T., Kitamura, N., et al., 2012. Vasopressin-induced intracellular Ca^{2+} concentration responses in non-neuronal cells of the rat dorsal root ganglion. Brain Res. 1483, 1–12.
Moriya, T., Shibasaki, R., Kayano, T., et al., 2015. Full-length transient receptor potential vanilloid 1 channels mediate calcium signals and possibly contribute to osmoreception in vasopressin neurones in the rat supraoptic nucleus. Cell Calcium 57, 25–37.
Neprasova, H., Anderova, M., Petrik, D., et al., 2007. Changes in voltage-dependent K^+ and Na^+ currents and volume regulation in astrocytes exposed to elevated K^+. Pflugers Arch. 453 (6), 839–849.
Noiseux, N., Borie, M., Desnoyers, A., et al., 2012. Preconditioning of stem cells by oxytocin to improve their therapeutic potential. Endocrinology 153, 5361–5372.
Resende, R.R., da Costa, J.L., Kihara, A.H., et al., 2010. Intracellular Ca2+ regulation during neuronal differentiation of murine embryonal carcinoma and mesenchymal stem cells. Stem Cells Dev. 19, 379–394.
Safford, K.M., Safford, S.D., Gimble, J.M., et al., 2004. Characterization of neuronal/glial differentiation of murine adipose-derived adult stromal cells. Exp. Neurol. 187, 319–328.
Sauer, H., Sharifpanah, F., Hatry, M., et al., 2011. NOS inhibition synchronizes calcium oscillations in human adipose tissue-derived mesenchymal stem cells by increasing gap-junctional coupling. J. Cell. Physiol. 226, 1642–1650.
Scicchitano, B.M., Spath, L., Musaro, A., et al., 2005. Vasopressin-dependent myogenic cell differentiation is mediated by both Ca2+/calmodulin-dependent kinase and calcineurin pathways. Mol. Biol. Cell 16, 3632–3641.
Shinoda, K., Luijten, I.H., Hasegawa, Y., et al., 2015. Genetic and functional characterization of clonally derived adult human brown adipocytes. Nat. Med. 21, 389–394.
Suzuki, H., Kawasaki, M., Ohnishi, H., et al., 2009. Exaggerated response of a vasopressin-enhanced green fluorescent protein transgene to nociceptive stimulation in the rat. J. Neurosci. 29, 13182–13189.
Syed, N., Kennedy, C., 2012. Pharmacology of P2X receptors. Wiley Interdiscip. Rev. Membr. Transp. Signal. 1, 16–30.
Todoroki, M., Fujihara, H., Otsubo, H., et al., 2010. Induction of the arginine vasopressin-enhanced green fluorescent protein fusion gene in the locus coeruleus in these transgenic rats. Stress 13, 281–291.
Tran, T.D., Yao, S., Hsu, W.H., et al., 2015. Arginine vasopressin inhibits adipogenesis in human adipose-derived stem cells. Mol. Cell. Endocrinol. 406, 1–9.
Ueta, Y., Fujihara, H., Dayanithi, G., et al., 2008. Specific expression of optically active reporter gene in arginine vasopressin-secreting neurosecretory cells in the hypothalamic-neurohypophyseal system. J. Neuroendocrinol. 20, 660–664.
Viero, C., Forostyak, O., Sykova, E., et al., 2014. Getting it right before transplantation: example of a stem cell model with regenerative potential for the cns. Front. Cell. Dev. Biol. 2, 36.
Viero, C., Mechaly, I., Aptel, H., et al., 2006. Rapid inhibition of Ca2+ influx by neurosteroids in murine embryonic sensory neurones. Cell Calcium 40, 383–391.
Viero, C., Shibuya, I., Kitamura, N., et al., 2010. Review: oxytocin: crossing the bridge between basic science and pharmacotherapy. CNS Neurosci. Ther. 16, e138–e156.
Wen, L., Wang, Y., Wang, H., et al., 2012. L-type calcium channels play a crucial role in the proliferation and osteogenic differentiation of bone marrow mesenchymal stem cells. Biochem. Biophys. Res. Commun. 424, 439–445.
Willingham, M.C., Pastan, I., 1975. Cyclic amp and cell morphology in cultured fibroblasts. Effects on cell shape, microfilament and microtubule distribution, and orientation to substratum. J. Cell Biol. 67, 146–159.
Yang, X.D., Zhao, L.Y., Zheng, Q.S., et al., 2003. Effects of arginine vasopressin on growth of rat cardiac fibroblasts: role of v1 receptor. J. Cardiovasc. Pharmacol. 42, 132–135.
Ye, B., 2010. Ca2+ oscillations and its transporters in mesenchymal stem cells. Physiol. Res. 59, 323–329.
Zhu, T., Yu, D., Feng, J., et al., 2015. Gdnf and nt-3 induce progenitor bone mesenchymal stem cell differentiation into neurons in fetal gut culture medium. Cell. Mol. Neurobiol. 35, 255–264.
Zippel, N., Limbach, C.A., Ratajski, N., et al., 2012. Purinergic receptors influence the differentiation of human mesenchymal stem cells. Stem Cells Dev. 21, 884–900.